Development of an intraventricular Adeno-Associated Virus-based labelling strategy for glioblastoma cells nested in the subventricular zone.

Arnaud Lombard[1,2†], Damla Isci[1†], Gilles Reuter[2,3], Emmanuel Di Valentin[4], Alexandre Hego[5], Didier Martin[2,3], Bernard Rogister[1,6], Virginie Neirinckx[1]

[1] Laboratory of Nervous System Diseases and Therapy, GIGA Neuroscience, University of Liège, Belgium.

[2] CHR Citadelle, Neurosurgery Department, Liège, Belgium

[3] University Hospital, Neurosurgery Department, Liège, Belgium

[4] GIGA Viral Vectors Platform, University of Liège, Belgium

[5] GIGA Cell Imaging Platform, University of Liège, Belgium

[6] University Hospital, Neurology Department, Liège, Belgium

† These authors contributed equally to this work.

Corresponding author

Virginie Neirinckx ; GIGA Neurosciences - Tour 4 (B36) Quartier Hôpital Avenue Hippocrate 15 B-4000 Liège ; +32 4 366 36 70 ; virginie.neirinckx@uliege.be

Conflict of Interest Statement

None declared

Fundings

This work is supported by the Fond National de la Recherche Scientifique (FNRS), the TELEVIE, the University of Liège and the Fondation Léon Frédéricq.

Authorship statement

AL, EDV, BR, VN: Study design. DM, BR, VN: Project supervision. AL, GR, DM: Tissue collection. AL, DI, AH: Experimental work. AL, DI, AH: Data analysis. AL, DI: Initial draft writing. AL, DI, AH, EDV, GR, DM, BR, VN: Review and final draft writing. All authors read and approved the final manuscript.

Abstract

Background

Glioblastoma (GBM) is a dreadful brain tumor, with a particular relationship to the adult subventricular zone (SVZ) that has been described as relevant to disease initiation, progression, and recurrence.

Methods

We propose a novel strategy for the detection and tracking of xenografted GBM cells that locate in the SVZ, based on an intracerebroventricular (icv) recombinant adeno-associated virus (AAV)-mediated color conversion method. We used different patient-derived GBM stem-like cells (GSCs), which we transduced first with a retroviral vector (LRLG) that included a lox-dsRed-STOP-lox cassette, upstream of the eGFP gene, then with rAAVs expressing the Cre-recombinase. Red and green fluorescence is analyzed *in vitro* and *in vivo* using flow cytometry and fluorescence microscopy.

Results

After comparing the efficiency of diverse rAAV serotypes, we confirmed that the *in vitro* transduction of GSC-LRLG with rAAV-Cre induced a switch from red to green fluorescence. In parallel, we verified that rAAV transduction was confined to the walls of the lateral ventricles. We therefore applied this conversion approach in two patient-derived orthotopic GSC xenograft models, and showed that the icv injection of an rAAV-DJ-Cre after GSC-LRLG tumor implantation triggered the conversion of red GSCs to green, in the periventricular region. Green GSCs were also found at distant places, including the migratory tract and the tumor core.

Conclusions

This study not only sheds light on the putative outcome of SVZ-nested GBM cells, but also shows that icv injection of rAAV vectors allows to transduce and potentially modulate gene expression in hard-to-reach GBM cells of the periventricular area.

Keywords

Glioblastoma, subventricular zone, SVZ-nested GBM cells, adeno-associated virus, intracerebroventricular

Key points

- This study details a new AAV-based method to specifically detect and track glioblastoma cells that nest in the subventricular zone.
- GBM cells nesting in the SVZ shortly leave this region to migrate towards other brain areas, including the initial tumor core.

Importance of the study

Many studies support that the adult subventricular zone (SVZ) can be considered as a specific niche allowing glioblastoma (GBM) initiation, progression, and recurrence. In this context, we aimed to develop a new strategy to label and track the SVZ-nested GBM cells in a preclinical patient-derived orthotopic xenograft model. Such tools that allow to reliably detect hard-to-reach GBM cells in the SVZ will help to shed light on their contribution to disease progression and relapse, and open new perspectives on the genetic modulation of these SVZ-nested cells in a therapeutic context.

1. Introduction

Glioblastoma (GBM) is the most frequent malignant brain tumor with dismal prognosis. After a maximal safe debulking surgery and subsequent radio-chemotherapy[1], tumors repeatedly relapse, typically in the margin of the resection cavity but also at more distant places[2]. This secondary progression of the disease seems to originate from the persistence of tumor cells that escaped surgery, resisted treatment, and initiated new tumor formation. Those specific features have classically been associated with GBM stem-like cells (GSCs), long considered as significant actors in tumor maintenance and recurrence[3].

The subventricular zone (SVZ) is a neurogenic area in the adult mammalian brain, running along the lateral walls of lateral ventricles (LV)[4]. Adult neural stem cells (NSCs) that locate in this region have been extensively characterized in mice, and were also detected in the SVZ of the adult human brain[5]. Increasing clinical evidence highlighted that the proximity of GBM tumors with the SVZ was associated with greater tumor invasiveness[6] and poor prognosis[7–9]. Different studies demonstrated that the accumulation of mutations in SVZ NSCs result in glioma initiation in genetically engineered mouse models[10,11]. In 2018, Lee et al. demonstrated that NSCs carrying low-level driver gene mutations (e.g. *TP53*, *PTEN*, *EGFR* and *TERT*) are detected in the SVZ of GBM patients, and match with the mutational burden of the tumors. They also used genetic models to show that NSCs with key driver mutations migrate out of the SVZ and develop GBM-like tumors at distant areas[12].

Using glioma patient-derived orthotopic xenograft (PDOX) models, we and others previously revealed glioma cell chemoattraction and infiltration within the SVZ[13,14]. These SVZ-nested GBM cells display stem-like features[15], and show modified sensitivity to ionizing radiation (IR)[16]. Another study suggested that SVZ-nested GBM cells support tumor resistance to chemotherapy[17]. As a whole, these data point out the key contribution of the SVZ in GBM initiation and progression, and putatively in GBM recurrence.

In this context, we aimed to establish an experimental model to specifically detect and tract SVZ-nested GBM cells in a PDOX setting. We designed a model that consists in the engraftment of patient-derived GBM stem-like cells (GSCs) that are initially red, and conditionally turn green upon invasion in the SVZ where they would be transduced by an adeno-associated viral (AAV) vector. AAVs are small, non-pathogenic single-stranded DNA (ssDNA) viruses and recombinant

AAV (rAAV) vectors have been extensively tested as gene delivery carriers in experimental as well as clinical investigations. In our approach, GSCs were transduced with a retroviral vector including a floxed dsRed/STOP cassette, upstream of the eGFP gene. Upon intracerebroventricular (icv) injection of rAAV delivering the Cre recombinase in the periventricular areas, the floxed dsRed/STOP cassette is excised to allow the expression of eGFP. In this study, we first validated the rAAV-mediated color conversion *in vitro*, and further showed how SVZ-nested GSCs can be detected and tracked *in vivo*, using regular microscopy but also tridimensional lightsheet microscopy after brain tissue clarification. Altogether, these results validate the establishment of an rAAV-based tracking method of GSCs that relocate in the SVZ, and pave the way for further investigation of the SVZ role in GBM biology.

2. Materials and Methods

2.1. Cell culture

Patient-derived GBM stem-like cells (GSCs) (GB1[18,19], T033 and T049) were established from residual tumor tissue after surgical resection, in collaboration with the Neurosurgery department of the Liège University Hospital (CHU), and the University Hospital Biobank (BHUL, Liège, Belgium), in accordance with the legal regulations on residual human body material. Relevant data on T033 and T049 patients and GSC cultures are found in Table S1).

GSCs were cultured as neurospheres in serum-free medium, consisting of DMEM/F12 containing 1x B27 without vitamin A (Thermo Fisher), 1% Penicillin-Streptomycin and supplemented with recombinant human epidermal growth factor (EGF) 20 ng/mL, and recombinant human fibroblast growth factor 2 (FGF-2), 10 ng/mL (Preprotech). For two-dimensional cultures, GB1 cells were cultured in DMEM supplemented with 5% fetal bovine serum (FBS) (Lonza) for the time of the experiment. Mycoplasma tests were performed on a regular basis. In culture, cells were maintained in a 5% CO_2 humidified incubator, at 37°C.

2.2. Viral vector production

Production of the LRLG retroviral vector: HEK-293T cells were co-transfected together with gene transfer plasmid pMSCV-lox-dsRed/STOP-lox-eGFP-Puro-WPRE [LRLG, Addgene plasmid # 3270][20], packaging plasmid [CellBiolabs # RV-111] and a VSV-G encoding plasmid. Retroviral supernatants were collected, concentrated, filtrated (0.22 µM) and used to transduce GB1, T033 and T049 cells.

Production of recombinant adeno-associated viral (rAAV) vectors: Briefly, pAAV-CMV-mRFP1, pAAV-EF1A-Cre-T2A-eYFP or pAAV-EF1a-Cre plasmids were co-transfected into 293AAV Cell Line (Cell Biolabs, AAV-100) together with a helper plasmid (Part No. 340202 VPK-401 kit) and REP-Cap plasmid (various serotypes: pAAV-1, pAAV-2, pAAV-5, pAAV-8, pAAV-9, pAAV-10[21] and pAAV-DJ, an artificial capsid that was generated by DNA family shuffling technology). After collection of the cell supernatant, rAAV vectors were titrated using ABM good kit (#GE931) at a concentration of 1E+12 genome copy/mL (GC/mL) (see Supplementary methods).

2.3. rAAV transduction of GSCs and flow cytometry analysis

For the screening of rAAV serotypes, 50.000 naïve GB1 cells were seeded in 6-well plates then cultured either in 2D or in 3D. After 6 hours, culture medium was supplemented with 2.5µL (2.5E+09gc) of rAAVs from different serotypes (1, 2, 5, 8, 9, 10, DJ), expressing RFP. After 72 hours, cells were collected in 500µL of PBS and RFP expression was analyzed using a Fortessa flow cytometer (BD Biosciences) and FlowJo software.

For the *in vitro* color conversion protocol, 50.000 GB1-LRLG, T033-LRLG and T049 cells were seeded in 6-well plates and supplemented with 2.5µL (2.5E+09gc) rAAV-DJ-Cre, rAAV-1-Cre or r-AAV-5-Cre. At day 3 or 7 of exposition, cells were collected in 500µL of PBS or maintained in culture for 7 additional days with fresh medium without rAAVs (to reach day 14). At each time point, cells were observed in live fluorescent imaging, DsRed and eGFP positivity was assessed by flow cytometry (Fortessa, BD Biosciences) and analyzed on FlowJo software.

2.4. Animal experiments

Intracranial transplantation of GSC-LRLG: Crl:NU-Foxn1^{nu} female mice were positioned in a stereotactic frame upon maintained isoflurane anesthesia. A hole was drilled on the skull bone (coordinates from bregma: 0.5 mm AP, +2 mm ML, 2.5 mm DV) and 50.000 GB1-LRLG or 100.000 T033-LRLG cells suspended in 2 µl PBS were injected into the right striatum, as previously described[22].

Intraventricular rAAV injection: At 1 week or 4 weeks post-transplantation, a hole was drilled on the skull bone. Then, 1 µL (1E+09gc) of rAAV-DJ-Cre-eYFP (to evaluate virus spreading without tumor) or rAAV-DJ-Cre (to excise the floxed cassette in tumor cells) were injected into the left lateral ventricle (coordinates from bregma: 0.2 mm AP, +0.8 mm ML, 2 mm DV). The needle was left in place for 2 minutes to prevent backflow before withdrawal.

2.5. Brain tissue processing

Mice were anaesthetized with an injection of Nembutal® (Pentobarbital 60 mg/mL, Ceva Sante Animal) before an intracardiac perfusion with NaCl 0.9% (VWR International) followed by ice-cold PFA 4% in PBS. Brains were collected, postfixed in 4% PFA overnight at 4°C and then conserved in PBS at 4°C for a maximum of 7 days.

Brain tissue clearing: Clarification of the right and left half-brains was performed as described before[23]. First, a 4°C-cocktail of hydrogel monomers (acrylamide with bisacrylamide), formaldehyde and thermally triggered initiators is infused into the tissue, for 24 hours. Then, the hydrogel polymerization is triggered at 37°C for 3 hours, followed by brain extraction and washing in borate-buffered 4% sodium-dodecyl-sulfate (SDS) solution at 37°C for 24h. After that, the brain is cleared using X-Clarity™ Tissue Clearing System II in an Electrophoretic Tissue Clearing Solution for 24 hours at room temperature, to remove the lipids without losing native tissue components. The resulting lipid-extracted and structurally stable tissue–hydrogel hybrid is then washed in PBS with 0,1% of Triton X-100, for 2 days at room temperature, and finally stored in PBS-azide at 4°C. Then, half-brains are immersed in a refractive index (RI) homogenization solution (Refractive Index Matching Solution; RI~1.460) to render it transparent to light.

Lightsheet microscopy: Half-brain images were acquired with a dual illumination lightsheet Z1 fluorescence microscope (Zeiss), equipped with a 5x/0.16 NA dry objective at a zoom of 0.36. Samples

were illuminated with 515 nm at 15%, 561 nm at 20% and 638 nm at 15% lasers. 1240 x 1240 pixel images (scaling x,y = 2.538 µm) were acquired using 2 sCMOS (pco.edge) camera with 30 ms exposure time. For Z-stack imaging, between 500 and 650 slices were acquired with a 9 µm z-step size. Images were stitched and reconstructed using Arivis Vision 4D software. Images were analyzed using Imaris (version 9.0) software and referenced using Allen Mouse Brain Atlas. To determine the distance between the LV and the transduced cells in the CP, we reconstructed the whole volume of the LV by contouring it on serial coronal sections (every 10μm) and measured the distance to the surface of the reconstructed LV volume.

2.6. Immunostainings

Immunohistochemistry and fluorescence on brain sections: Brain tissue was processed as described above. 14 µm-thick coronal brain slices were generated with a cryostat and stored at -20°C. Xenografted T033-LRLG cells were detected with human Vimentin antibody, with the Enzo PolyView IHC kit, according to the manufacturer's instructions. Brain slices were permeabilized and blocked with PBS + 0,3% Triton-X100 + 10% donkey serum for 1 hour and then incubated with anti-eGFP antibody overnight at 4°C. After washing steps with PBS, slides were incubated for 1 hour with Cy5-conjugated secondary antibody, to ensure the specificity of the signal (Jackson ImmunoResearch Laboratories). Antibodies against Ki67 and SOX2 were used for costainings. Nuclei were counterstained with DAPI (Sigma). Image acquisition was performed with an epifluorescence microscope (Zeiss Apotome) and analyzed on ImageJ (Fiji) software (see Supplementary methods).

Immunofluorescence on cells: 20.000 GB1 cells were transduced with rAAVs expressing RFP (serotypes 1, 2, 5, 8, 9, 10 and DJ). After 72 hours, cells were fixed with paraformaldehyde (PFA) 4%, and incubated with anti-RFP antibody diluted in PBS + 0.1% donkey serum and 0.1% Triton X-100, followed by a second incubation with Rhodamine red X-conjugated antibodies (Jackson Immunoresearch Laboratories). Nuclei were counterstained with Hoescht (Thermo Fisher Scientific cat#62249), and images were acquired with a Zeiss AxioImager Z1 epifluorescence microscope (see Supplementary methods).

2.7. Statistics

Statistics were realized thanks to GraphPad Prism v8. Normality was assessed by a Shapiro-Wilk test and either Student-t test, one-way ANOVA or 2way ANOVA were performed for group comparisons. Statistical significance was set at 0.05. Data are indicated as mean +/- standard deviation, with the number of independent experiments/animals indicated as N in the figure legends.

2.8. Study approval

Patient tissue was obtained in collaboration with the Neurosurgery department of the Liège University Hospital (CHU), and the University Hospital Biobank (BHUL, Liège, Belgium), in accordance with the legal regulations on human body material. This study was approved by the local human ethics committee.

Crl:NU-Foxn1^{nu} female mice were purchased at Charles River laboratories, housed in group of four individuals (ZT0: 7am, ZT12: 7pm). Mice health status was evaluated daily, and body weight was recorded every week. Tumor endpoint and animal sacrifice was considered at the first signs of significant discomfort or suffering. No mice had to be sacrificed at an early timepoint in this study. All animal experiments were approved by the ethical committee of the University of Liège (local protocol number 1737).

3. Results

3.1. In vitro assessment of rAAV transduction efficiency using diverse serotypes

First, we determined the efficiency of various AAV serotypes in transducing patient-derived GSCs *in vitro*. As a first screening, GB1 cells were infected with rAAVs from seven different serotypes (rAAV-1, rAAV-2, rAAV-5, rAAV-8, rAAV-9, rAAV-10 and rAAV-DJ) all expressing the red fluorescent protein (RFP), and then analyzed by flow cytometry (**Fig1, A**). In 2D-culture conditions, the percentage of RFP$^+$ GB1 cells after three days was higher than 50% with rAAV-1 (97.78±1,77%), rAAV-5 (67.23±4,42%) and rAAV-DJ (60,09±1,29%). In contrast, the transduction efficiency was significantly reduced for rAAV-2, rAAV-8, rAAV-9, rAAV-10 ($p<0,0001$) (**Fig1, B & FigS1 A,C**). When GB1 cells were cultured in 3D neurospheres, the percentage of RFP$^+$ tumor cells was again higher for rAAV-1 (64,69±5,1%), rAAV-5

(56,98±4,1%) and rAAV-DJ (60,11±8,3%), with again a significantly reduced transduction for rAAV-2, -8, -9, and -10 (p-values ranging from <0.05 to <0,001) (**Fig1, C & FigS1, B-C**). Those results were confirmed with an anti-RFP immunostaining performed on coated GB1 cells after three days of exposition to rAAV-1, rAAV-5 and rAAV-DJ (**Fig1, C**). Altogether, we concluded that rAAV-1, rAAV-5 and r-AAV-DJ are the most efficient serotype for GSC transduction *in vitro*.

3.2. In vitro validation of rAAV-Cre-mediated color conversion of GSC-LRLG

Prior to applying the red-to-green conversion in an *in vivo* setting, we verified the ability of the rAAV serotypes 1, 5 and DJ to induce such conversion in patient-derived GSCs in culture. T033, T049 and GB1 GSCs were stably transduced with a retroviral vector including a floxed dsRed/STOP cassette, upstream of the eGFP gene (LRLG vector). T033-LRLG, T049-LRLG and GB1-LRLG were further exposed to rAAV-1-Cre, rAAV-5-Cre or rAAV-DJ-Cre (**Fig2, A**).

Globally, all rAAV serotypes induced a progressive color conversion of T033-LRLG, from $dsRed^+$ (red) to $dsRed^+/GFP^+$ (orange) and finally $eGFP^+$ only (green) (**Fig2, B-E**). At 14 days, the rAAV-DJ-Cre induced 75,92±5,24% $eGFP^+$ cells in T033-LRLG, which is significantly higher than rAAV-5-Cre (56,87±4,20%; p=0.0193), and slightly increased compared to rAAV-1-Cre (62,99±10,91%; p=0.0309). The % of $eGFP^+$ cells was significantly higher at day 14 compared to day 7 in rAAV-DJ-Cre transduced T033-LRLG (p=0.0314) (**Fig2, F-G**). A similar time-dependent color conversion was observed upon transduction of T049-LRLG with the three rAAV serotypes (**Fig2, H-J**). The rAAV-DJ-Cre induced 81,78±5,42% $eGFP^+$ cells at day 14, while lower number of eGFP+ were induced with rAAV-5-Cre (66,45±11,39%; p=0.2419), and with rAAV-1-Cre (69;49±6,36%; p=0.1324). Again, the % of $eGFP^+$ cells was significantly higher at day 14 compared to day 7 in rAAV-DJ-Cre transduced T049-LRLG (p=0.0027) (**Fig2, K-L**). We also tested the rAAV-DJ-Cre in GB1-LRLG and observed a progressive increase of $eGFP^+$ cells, reaching 63.36±0.14% at day 14 (**Fig S1, D-E**). Based on these results, we concluded that the three rAAV serotypes adequately transduce GSC-LRLG and induce red-to-green conversion *in vitro*, with the rAAV-DJ emerging as the most efficient.

3.3. Dissemination of rAAV-Cre-eYFP after icv injection in the naïve brain

After injection in the brain, the dissemination of the AAV-DJ serotype is reported as more confined compared to other serotypes[21]. Here, we wanted to evaluate the spreading of rAAV-Cre vectors upon intracerebroventricular (icv) injection, to assess whether rAAV transduction would be restricted to the walls of the lateral ventricles. rAAV-1-Cre-eYFP, rAAV-5-Cre-eYFP and rAAV-DJ-Cre-eYFP were icv injected in naïve nude mice (n=3 mice per group), and brains were collected 1 week after injection. Imaging of the brain sections showed that eYFP signal is tightly limited to the borders of the lateral ventricles (**Fig3, A**), which would ensure that rAAV transduction of GBM cells in a xenograft model would be restricted to cells within the SVZ.

Furthermore, we could analyze mice that were icv injected with rAAV-DJ-Cre-eYFP, at 4 weeks post-injection, after brain tissue clearing and lightsheet microscopy, to precisely quantify rAAV spreading at longer term. We determined the volume of YFP-positive signal for different regions adjoining the lateral (LV) and the third (V3) ventricles (n=5 mice) (**Fig3, B**). Medially to the LV, we observed YFP-positive signal in the Lateral Septal nucleus (LSc) (**Fig3, B-C,** *yellow arrow*). Laterally to the LV, YFP-positive signal was detected in a few layers of cells in the SVZ and in the medial part of the caudoputamen (mCP), anteriorly (**Fig3, B-C,** *orange arrow*) and in its dorsolateral part (dlCP), posteriorly (**Fig3, B-C,** *purple arrow*). In the nearby of LV posterior wall, we also highlighted the transduction of few cells in the fimbria (Fi) (**Fig3, B-C,** *red arrow*) and in the Ammon's horn of the hippocampus (HPF), where the YFP^+ area was the larger (**Fig3, B,-C** *green arrow*). Some isolated cells in the corpus callosum (CC) (**Fig3, B-C,** *grey arrow*) were also detected. The YFP^+ area was significantly higher in the HPF compared to the mCP ($p=0.0409$), to the Fi ($p=0.0236$) and to the CC ($p=0.0268$), which suggests that cells are more likely transduced in structures enriched in neuronal bodies (HPF, LSc, CP), rather than in white matter tracts (Fi, CC). Finally, we measured the longest distance between the LV and the transduced cells in the mCP (P25<median<P75: 128,75<162,5<182μm) and in the dlCP (210μm-294μm-531,67μm) (**Fig3, D**). This data shows that 4 weeks after injection, the rAAV-DJ-C-eYFP spreads towards other structures distant from the LV, although below five hundred micrometers.

3.4.In vivo validation of rAAV-Cre-mediated color conversion of GSC-LRLG that invaded the subventricular zone (SVZ)

Previous work from our group has shown that GB1-LRLG cells form a symptomatic tumor upon implantation in the striatum of nude mice within 12 to 16 weeks, associated to an invasion of the subventricular zone (SVZ)[22]. Hence, we icv injected the rAAV-DJ-Cre at week 6 after GB1-LRLG cell engraftment, before SVZ invasion (group I, n=8 mice), and at week 12, after SVZ invasion (group II, n=8 mice). We finished the experiment 4 weeks later, respectively at week 10 (group I) and at week 16 (group II) (**Fig4, A**). Brain tissue was cleared, and the right hemispheres were imaged with a lightsheet microscope, and analyzed with Imaris® software, for highlighting $dsRed^+$ and $eGFP^+$ tumor cells. As expected, the median volume of dsRed-positive tumors in the CP was reduced in group I μm^3 (P25<median<P75: 2.40<5.73<6.66 $x10^7 \mu m^3$) compared to group II (2.23<9.88<2.23$x10^9 \mu m^3$) (p=0.0016) (**Fig4, B-C**). In group I, we did not observe any contact of the tumor with the SVZ and no $eGFP^+$ signal was detected (**Fig4, B-D**). However, we observed eGFP+ signal in most animals from group II (volume of P25<median<P75: 1.25<5.88<9.74 $x10^6 \mu m^3$), especially those with the largest dsRed+ tumor volume (R^2:0.58, p=0.0267) (**Fig4, D-E**).

We also tested the ability of the rAAV-DJ-Cre to promote red-to-green conversion in another GSC intrastriatal xenograft, within a different timeframe. At 6 weeks, T033-LRLG cells establish a large infiltrating tumor that invade both the right and left LV lateral walls via the corpus callosum (**FigS2**). The rAAV-DJ-Cre was icv injected in the left LV at week 5 post-engraftment (**Fig5, A**). One week later, mice were sacrificed, and brains collected. Immunostainings showed $dsRed^+$ T033-LRLG cells scattered in the right hemisphere, as well as in the right and left LV. Not only are $eGFP^+$ cells detected near the left LV, but also in the proximity of the right LV and within the tumor core (**Fig5, B-C**). These eGFP+ cells are $SOX2^+$ and $Ki67^+$, which indicates a maintained potential for proliferation (**Fig6**). These results support the hypothesis that $dsRed^+$ tumor cells develop and migrate out of the tumor mass to reach the LV walls, where they switch from $dsRed^+$ to $eGFP^+$. Interestingly, these eGFP+ cells appear to leave the LV and reinfiltrate the initial tumor core. In absence of tumor cells in the LV surroundings (i.e. for tumors that did not grow sufficiently large), we did not see any $eGFP^+$ cell at all (**FigS3**), which is in line with the restricted diffusion of the rAAV and further supports the specificity of the SVZ-located transduction. Altogether, these

results demonstrate the relevance of an icv AAV-based color conversion approach to detect GBM cells that invade the LV wall/SVZ. These results also shed light on the putative role of SVZ-nested GBM cells in tumor evolution and recurrence.

4. Discussion

Many studies have evidenced the key contribution of the subventricular zone (SVZ) of the adult brain in glioblastoma (GBM) initiation, maintenance and recurrence. At the clinical level, the proximity of GBM tumors with the SVZ (SVZ^+ GBM) has been associated with worse prognosis[7–9], and different experimental findings have demonstrated the protective role of the SVZ environment against therapy[16,17]. SVZ^+ GBM is associated to particular methylation signatures[24], and recent single cell transcriptomic data suggest a differential cell type enrichment and related therapeutic vulnerabilities[25]. Such data fosters deeper investigation of the molecular mechanisms that underlie the influence of SVZ environment on GBM cell fate and phenotype, and the development of experimental tools to do so. In this study, we harnessed different types of viral vectors to label and track GBM cells invading the SVZ in an orthotopic xenograft model. Using a color-conversion approach, we observed that implanted $dsRed^+$ patient-derived GBM stem-like cells (GSCs) do infiltrate the brain and reach the SVZ where they turn $eGFP^+$, with the help of a recombinant adeno-associated viral (rAAV) delivering a Cre recombinase inside the lateral ventricle. To our knowledge, this study proposes an original approach to study SVZ-nested GBM cells, and also is the first to suggest that GBM cells nesting in the SVZ may actually leave this region to repopulate other brain areas. Of note, this experimental strategy is versatile, and the SVZ-restricted color-conversion approach could be further refined.

Whereas a similar LRLG vector-based method has previously been used for monitoring transduction efficiency[26], or for lineage tracing[27], other studies further exploited this strategy, to monitor environmental influences on cancer cells, i.e. for fate-mapping post-hypoxic breast cancer cells and investigating their phenotype and role in the metastatic process, using a HIF1α-dependent expression of Cre recombinase[28,29]. Such conditional Cre expression may also be applied and highly relevant in the exploration of SVZ molecular influences on GBM cells. For example, it would be interesting to use a Cre recombinase that would be dependent on a particular component

in the cerebrospinal fluid, or in the SVZ vasculature, to assess how these are influencing GBM cells nested in the periventricular area.

The many natural and engineered rAAV capsid serotypes that are reported or under ongoing development have distinct but overlapping tropisms and distribution [30,31]. Whereas we here selected AAV-DJ as an efficient serotype for GSC transduction among a panel of AAV serotypes, other novel rAAV constructs may be envisaged for specific properties, e.g. restricted surface of action, or more specific GBM cell transduction. A recent high-throughput screening of 177 AAV capsid variants has shown that AAV1-P5 most effectively transduces NSCs in the naïve adult brain after icv injection, and these can be tracked up to their final destination in the olfactory bulb[32]. The AAV-SCH9 also efficiently transduces adult NSCs[33]. To what extent this NSC-oriented tropism would be recapitulated on SVZ-nested GSCs remains to be investigated.

The transgene of interest may also be replaced, e.g. for modulating gene expression in the target cells in a therapeutic purpose, for inducing cell death, reducing proliferation or stimulating immune recognition. For instance, AAV intraventricular injection has already been described in GBM models, e.g for the delivery of interferon γ (IFNγ). A first report show that icv AAV2/rh8-IFNγ preferentially distributes in the corpus callosum and the hippocampus, similar to what we observed here with AAV-DJ (at lower viral titration), and reduces tumor growth in a U87 model[34]. Later, they showed that icv AAV9-IFNγ reduced tumor growth and increases survival in an invasive patient-derived xenograft model, as well as in an immunocompetent model, and synergizes with temozolomide treatment[35]. AAV9 armed with the sTRAIL proapoptotic protein has also shown promising therapeutic effect in GBM models, upon systemic injection[36]. It would be of huge interest to induce therapeutic genes in SVZ-nested GBM cells to ascertain their contribution to tumor resistance to treatment and recurrence.

In addition to these molecular developments that could apply to this approach, we also point out the importance of considering clinically relevant, therapy-like models to be combined to our color-conversion protocol. For example, it would be interesting to observe whether eGFP+, SVZ-relocated GBM cells are able to repopulate an experimental resection cavity, for instance using microsurgery models[37].

Altogether, this work exposes the development of an rAAV-based approach for the specific and restricted labelling of GBM cells that get in close contact with the subventricular zone (SVZ), after tumor development in a xenograft mouse model. This experimental approach is highly

relevant to the clinical context describing the poor prognosis associated with GBM proximity to the SVZ. This versatile model could be optimized for both investigational and therapeutic perspectives and will help to shed light on the spatiotemporal aspects of GBM progression and recurrence.

5. Funding

This work is supported by the Fond National de la Recherche Scientifique (FNRS), the TELEVIE, the University of Liège and the Fondation Léon Frédéricq.

6. Authorship statement

AL, EDV, BR, VN: Study design. DM, BR, VN: Project supervision. AL, GR, DM: Tissue collection. AL, DI, AH: Experimental work. AL, DI, AH: Data analysis. AL, DI: Initial draft writing. AL, DI, AH, EDV, GR, DM, BR, VN: Review and final draft writing. All authors read and approved the final manuscript.

7. Conflict of Interest Statement

None declared

8. Acknowledgements

We thank the colleagues from the GIGA-Viral Vector platform, the Neurosurgery Department the University Hospital Biobank. Plasmids pAAV8, pAAV9, pAAV10 were kind gifts from Miguel Sena-Esteves (UMass Chan Medical School). The plasmid pMSCV-loxp-dsRed-loxp-eGFP-Puro-WPRE was a gift from Hans Clevers (Addgene plasmid #32702; http://n2t.net/addgene:32702 ; RRID:Addgene_32702).

9. Data availability

The data are available from the corresponding author upon request.

10. References

1. Stupp R, Mason WP, van den Bent MJ, et al. Radiotherapy plus concomitant and adjuvant temozolomide for glioblastoma. *N Engl J Med*. 2005;352(10):987-996. doi:10.1056/NEJMOA043330

2. Rapp M, Baernreuther J, Turowski B, Steiger HJ, Sabel M, Kamp MA. Recurrence Pattern Analysis of Primary Glioblastoma. *World Neurosurg*. 2017;103:733-740. doi:10.1016/J.WNEU.2017.04.053

3. Ignatova TN, Kukekov VG, Laywell ED, Suslov ON, Vrionis FD, Steindler DA. Human cortical glial tumors contain neural stem-like cells expressing astroglial and neuronal markers in vitro. *Glia*. 2002;39(3):193-206. doi:10.1002/GLIA.10094

4. Alvarez-Buylla A, García-Verdugo JM. Neurogenesis in adult subventricular zone. *Journal of Neuroscience*. Published online 2002. doi:10.1523/jneurosci.22-03-00629.2002

5. Sanai N, Tramontin AD, Quinones-Hinojosa A, et al. Unique astrocyte ribbon in adult human brain contains neural stem cells but lacks chain migration. *Nature*. 2004;427(6976):740.

6. Lim DA, Cha S, Mayo MC, et al. Relationship of glioblastoma multiforme to neural stem cell regions predicts invasive and multifocal tumor phenotype. *Neuro Oncol*. Published online 2007. doi:10.1215/15228517-2007-023

7. Jafri NF, Clarke JL, Weinberg V, Barani IJ, Cha S. Relationship of glioblastoma multiforme to the subventricular zone is associated with survival. *Neuro Oncol*. 2013;15(1):91-96. doi:10.1093/NEUONC/NOS268

8. Mistry AM, Hale AT, Chambless LB, Weaver KD, Thompson RC, Ihrie RA. Influence of glioblastoma contact with the lateral ventricle on survival: a meta-analysis. *J Neurooncol*. 2017;131(1):125-133. doi:10.1007/S11060-016-2278-7

9. Adeberg S, Bostel T, König L, Welzel T, Debus J, Combs SE. A comparison of long-term survivors and short-term survivors with glioblastoma, subventricular zone involvement: A predictive factor for survival? *Radiation Oncology*. Published online 2014. doi:10.1186/1748-717X-9-95

10. Wang Y, Yang J, Zheng H, et al. Expression of mutant p53 proteins implicates a lineage relationship between neural stem cells and malignant astrocytic glioma in a murine model. *Cancer Cell*. 2009;15(6):514-526. doi:10.1016/j.ccr.2009.04.001

11. Alcantara Llaguno S, Sun D, Pedraza AM, et al. Cell-of-origin susceptibility to glioblastoma formation declines with neural lineage restriction. *Nature Neuroscience 2019 22:4*. 2019;22(4):545-555. doi:10.1038/s41593-018-0333-8

12. Lee JH, Lee JE, Kahng JY, et al. Human glioblastoma arises from subventricular zone cells with low-level driver mutations. *Nature*. Published online 2018:1.

13. Goffart N, Kroonen J, Di Valentin E, et al. Adult mouse subventricular zones stimulate glioblastoma stem cells specific invasion through CXCL12/CXCR4 signaling. *Neuro Oncol*. Published online 2015. doi:10.1093/neuonc/nou144

14. Qin EY, Cooper DD, Abbott KL, et al. Neural Precursor-Derived Pleiotrophin Mediates Subventricular Zone Invasion by Glioma. *Cell*. Published online 2017. doi:10.1016/j.cell.2017.07.016

15. Kroonen J, Nassen J, Boulanger YG, et al. Human glioblastoma-initiating cells invade specifically the subventricular zones and olfactory bulbs of mice after striatal injection. *Int J Cancer*. Published online 2011. doi:10.1002/ijc.25709

16. Goffart N, Lombard A, Lallemand F, et al. CXCL12 mediates glioblastoma resistance to radiotherapy in the subventricular zone. *Neuro Oncol*. Published online 2017. doi:10.1093/neuonc/now136

17. Piccirillo SGM, Spiteri I, Sottoriva A, et al. Contributions to drug resistance in glioblastoma derived from malignant cells in the sub-ependymal zone. *Cancer Res*. 2015;75(1):194-202. doi:10.1158/0008-5472.CAN-13-3131/651340/AM/CONTRIBUTIONS-TO-DRUG-RESISTANCE-IN-GLIOBLASTOMA

18. Willems E, Dedobbeleer M, Digregorio M, et al. Aurora A plays a dual role in migration and survival of human glioblastoma cells according to the CXCL12 concentration. *Oncogene*. Published online 2019. doi:10.1038/s41388-018-0437-3

19. Dedobbeleer M, Willems E, Lambert J, et al. MKP1 phosphatase is recruited by CXCL12 in glioblastoma cells and plays a role in DNA strand breaks repair. *Carcinogenesis*. Published online 2020. doi:10.1093/carcin/bgz151

20. Koo BK, Stange DE, Sato T, et al. Controlled gene expression in primary Lgr5 organoid cultures. *Nat Methods*. 2012;9(1):81.

21. Haery L, Deverman BE, Matho KS, et al. Adeno-Associated Virus Technologies and Methods for Targeted Neuronal Manipulation. *Front Neuroanat*. 2019;13. doi:10.3389/FNANA.2019.00093

22. Goffart N, Lombard A, Lallemand F, et al. CXCL12 mediates glioblastoma resistance to radiotherapy in the subventricular zone. *Neuro Oncol*. 2017;19(1):66-77. doi:10.1093/neuonc/now136

23. Tomer R, Deisseroth K. Advanced CLARITY Methods for Rapid and High-Resolution Imaging of Intact Tissues. Published online 2014.

24. Adeberg S, Knoll M, Koelsche C, et al. DNA-methylome-assisted classification of patients with poor prognostic subventricular zone associated IDH-wildtype glioblastoma. *Acta Neuropathologica 2022 144:1*. 2022;144(1):129-142. doi:10.1007/S00401-022-02443-2

25. Licón-Muñoz Y, Avalos V, Subramanian S, et al. Single-nucleus and spatial landscape of the sub-ventricular zone in human glioblastoma.

26. Schubert L, Le AT, Hinz TK, et al. A functional sgRNA-CRISPR screening method for generating murine RET and NTRK1 rearranged oncogenes. Published online 2023. doi:10.1242/bio.059994

27. Guo Y, Lei I, Tian S, et al. Chemical suppression of specific C-C chemokine signaling pathways enhances cardiac reprogramming. *Journal of Biological Chemistry*. 2019;294(23):9134-9146. doi:10.1074/JBC.RA118.006000/ATTACHMENT/EEC4CC7E-2357-425D-93E5-0568CBCEE9A5/MMC1.ZIP

28. Godet I, Shin YJ, Ju JA, Ye IC, Wang G, Gilkes DM. Fate-mapping post-hypoxic tumor cells reveals a ROS-resistant phenotype that promotes metastasis. *Nature Communications 2019 10:1*. 2019;10(1):1-18. doi:10.1038/s41467-019-12412-1

29. Rocha HL, Godet I, Kurtoglu F, et al. A persistent invasive phenotype in post-hypoxic tumor cells is revealed by fate mapping and computational modeling. *iScience*. 2021;24(9):102935. doi:10.1016/J.ISCI.2021.102935

30. Haery L, Deverman BE, Matho KS, et al. Adeno-Associated Virus Technologies and Methods for Targeted Neuronal Manipulation. *Front Neuroanat*. 2019;13:493120. doi:10.3389/FNANA.2019.00093/BIBTEX

31. Xu X, Chen W, Zhu W, et al. Adeno-associated virus (AAV)-based gene therapy for glioblastoma. *Cancer Cell Int*. 2021;21(1):1-10. doi:10.1186/S12935-021-01776-4/TABLES/2

32. Kremer LPM, Cerrizuela S, Dehler S, et al. High throughput screening of novel AAV capsids identifies variants for transduction of adult NSCs within the subventricular zone. *Mol Ther Methods Clin Dev*. 2021;23:33-50. doi:10.1016/J.OMTM.2021.07.001

33. Ojala DS, Sun S, Santiago-Ortiz JL, Shapiro MG, Romero PA, Schaffer D V. In Vivo Selection of a Computationally Designed SCHEMA AAV Library Yields a Novel Variant for Infection of Adult Neural Stem Cells in the SVZ. *Molecular Therapy*. 2018;26(1):304-319. doi:10.1016/J.YMTHE.2017.09.006/ATTACHMENT/C5A91BE4-4B73-4495-8A18-35FD1DC90D6B/MMC1.PDF

34. Meijer DH, Maguire CA, Leroy SG, Sena-Esteves M. Controlling brain tumor growth by intraventricular administration of an AAV vector encoding IFN-β. *Cancer Gene Therapy 2009 16:8*. 2009;16(8):664-671. doi:10.1038/cgt.2009.8

35. Guhasarkar D, Neiswender J, Su Q, Gao G, Sena-Esteves M. Intracranial AAV-IFN-β gene therapy eliminates invasive xenograft glioblastoma and improves survival in orthotopic syngeneic murine model. *Mol Oncol*. 2017;11(2):180-193. doi:10.1002/1878-0261.12020

36. Crommentuijn MHW, Kantar R, Noske DP, et al. Systemically administered AAV9-sTRAIL combats invasive glioblastoma in a patient-derived orthotopic xenograft model. *Mol Ther Oncolytics*. 2016;3:16017. doi:10.1038/mto.2016.17

37. Oudin A, Moreno-Sanchez PM, Baus V, Niclou SP, Golebiewska A. Magnetic resonance imaging-guided intracranial resection of glioblastoma tumors in patient-derived orthotopic xenografts leads to clinically relevant tumor recurrence. *BMC Cancer*. 2024;24(1):1-14. doi:10.1186/S12885-023-11774-6/FIGURES/5

11. Figure legends

Figure 1: rAAV-1, rAAV-5 and rAAV-DJ efficiently transduce patient-derived GBM stem-like cell (GSC) cultures. **(A)** Flowchart representing the rAAV-RFP transduction of GSCs for the screening of most efficient serotypes (created with BioRender®). **(B)** % GB1 cells expressing RFP in 2D-culture after a three-day exposition to rAAVs (n=3 independent experiments) (one-way ANOVA, p-values for each comparison in FigS1, A). **(C)** Immunofluorescent staining of the RFP protein (red) after rAAV-DJ-RFP transduction of GB1 cells (Scale bar = 50 µm). **(D)** % GB1 cells expressing RFP in 3D-culture after a three-day exposition to rAAVs (n=3 independent experiments) (one-way ANOVA, p-values for each comparison in FigS1, B).

Figure 2: **rAAV-1, rAAV-5 and rAAV-DJ efficiently convert GSC-LRLG cells in culture from dsRed$^+$ to eGFP$^+$.** **(A)** Flowchart representing of dsRed gene excision and fluorescent eGFP gene expression in GSCs induced by rAAV-mediated Cre recombinase (created with BioRender®). (**B**) Representative imagines of the dsRed and eGFP signals in T033-LRLG cultures transduced with rAAV-DJ-Cre, over 14 days. (**C-D-E**) % T033-LRLG cells that are found dsRed$^+$ (red), dsRed$^+$/eGFP+ (orange) or eGFP$^+$ only (green) at 3, 7 and 14 days post-transduction with rAAV-1-Cre (C), rAAV-5-Cre (D) and rAAV-DJ-Cre (E). (NT= non transduced, at day 0). (**F**) % eGFP$^+$ T033-LRLG cells over time, with the three rAAV serotypes (n=3 independent experiments). (**G**) Results from the 2way ANOVA, providing the statistical effect of the serotype and the effect of time. (**H-I-J**) % T049-LRLG cells that are found dsRed$^+$ (red), dsRed$^+$/eGFP+ (orange) or eGFP$^+$ only (green) at 3, 7 and 14 days post-transduction with rAAV-1-Cre (H), rAAV-5-Cre (I) and rAAV-DJ-Cre (J) (NT= non transduced, at day 0). (**K**) % eGFP$^+$ T049-LRLG cells over time, with the three rAAV serotypes (n=3 independent experiments). (**L**) Results from the 2way ANOVA, providing the statistical effect of the serotype and the effect of time.

Figure 3. The rAAV-DJ-Cre-eYFP has LV-restricted spreading 1 week after icv injection and disseminates to adjacent neuron-rich structures after 4 weeks. (**A**) rAAV-1-eYFP, rAAV-5-eYFP and rAAV-DJ-eYFP remain confined to the lateral ventricle walls one week after icv injection. Images are representative of n=3 mice per serotype tested (scale bars = 100 µm). (**B**) Sagittal views at the VL medial wall (400 µm laterally to Bregma), through the VL (1mm laterally to Bregma) and at the VL lateral wall (1500 µm laterally

to Bregma) to visualize YFP$^+$ cells (scale bars = 400µm). **(C)** Comparison of the volume (in μm^3) of YFP fluorescence in transduced areas in the LV neighboring (n=5 mice) (one-way ANOVA, p-values for each comparison in FigS2, A). **(D)** Longest distance (μm) between the further YFP$^+$ cells in the mCP and dlCP and the lateral wall of the VL (n=5). Legend: *LSc : lateral septal nucleus, mCP : medial caudoputamen, dlCP : dorsolateral caudoputamen, Fi : fimbria, CC : corpus callosum, HPF : hippocampus.*

Figure 4. rAAV-DJ-Cre icv injection induces red-to-green conversion of GB1-LRLG that reached the subventricular zone (SVZ) in an orthotopic xenograft model. (A) Flowchart representing the experimental workflow. GB1-LRLG cells were implanted in nude mice and rAAV-DJ-Cre-YFP was icv injected at week 6 (group I) or week 12 (group II). Then mice were sacrificed at week 10 or week 16 respectively. **(B)** Analysis of right hemispheres with a lightsheet microscope, highlighting dsRed and eGFP-positive tumor areas. **(C)** Quantification of the dsRed-positive tumor area in mice from groups I and II (Mann-Whitney U-test, n=8 mice per group). **(D)** Quantification of the eGFP-positive tumor area in mice from groups I and II (n=8 mice per group). **(E)** Correspondence between dsRed+ and eGFP+ volumes in group II animals (linear regression).

Figure 5. rAAV-DJ-Cre icv injection induces red-to-green conversion of T033-LRLG that reached the subventricular zone (SVZ) in an orthotopic xenograft model. (A) Flowchart representing the experimental workflow. T033-LRLG cells were implanted in nude mice and rAAV-DJ-Cre-YFP was icv injected intraventricularly at week 5, and mice were sacrificed at week 6. **(B-C)** Immunofluorescence stainings of eGFP+ (green) and dsRed+ (red) cells in different regions of the mouse brain (right striatum, right lateral ventricle, left lateral ventricle). Sections of three different animals are displayed (scale bar = 50 or 100 μm).

Figure 6. Characterization of eGFP+ T033-LRLG cells. Immunofluorescence costainings of SOX2 and Ki67 (white) with eGFP+ (green) and dsRED+ (red) cells in different regions of the mouse brain implanted with T033-LRLG and one week after rAAV-DJ-Cre icv injection. Sections of three different animals are displayed (scale bar = 100 μm).

Figure 1

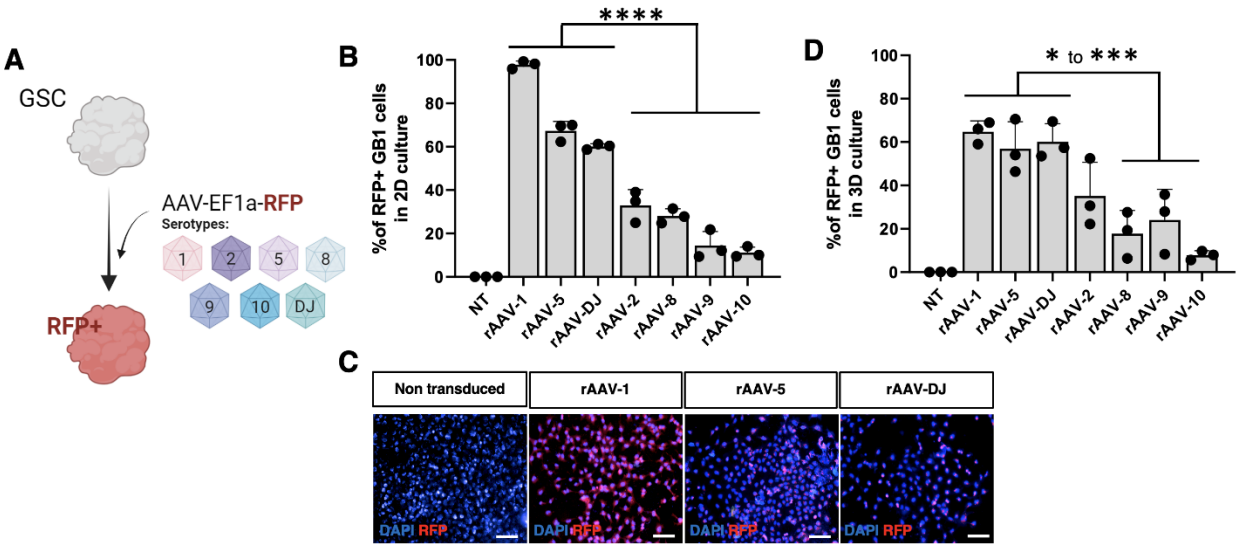

Figure 2

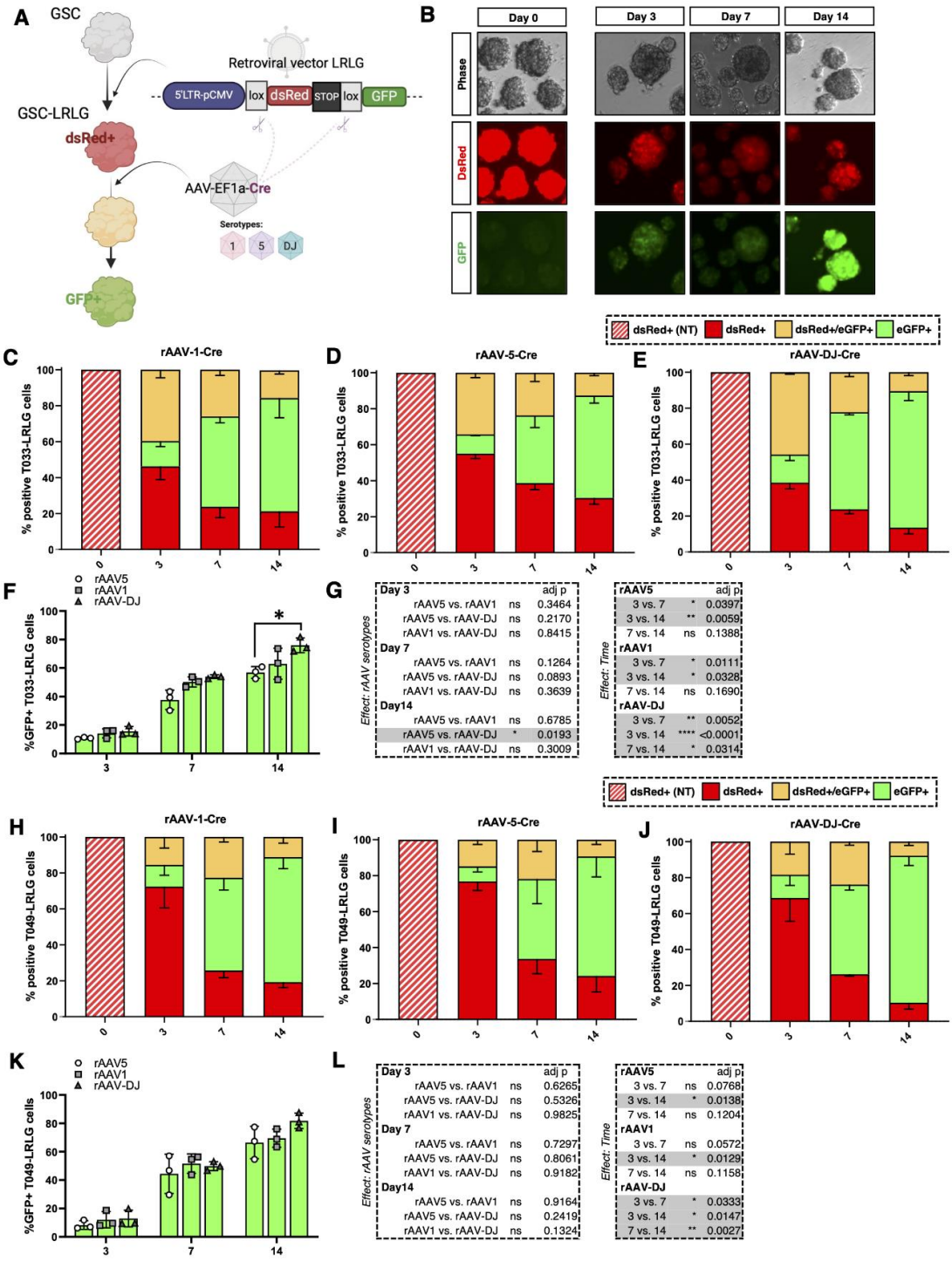

Figure 3

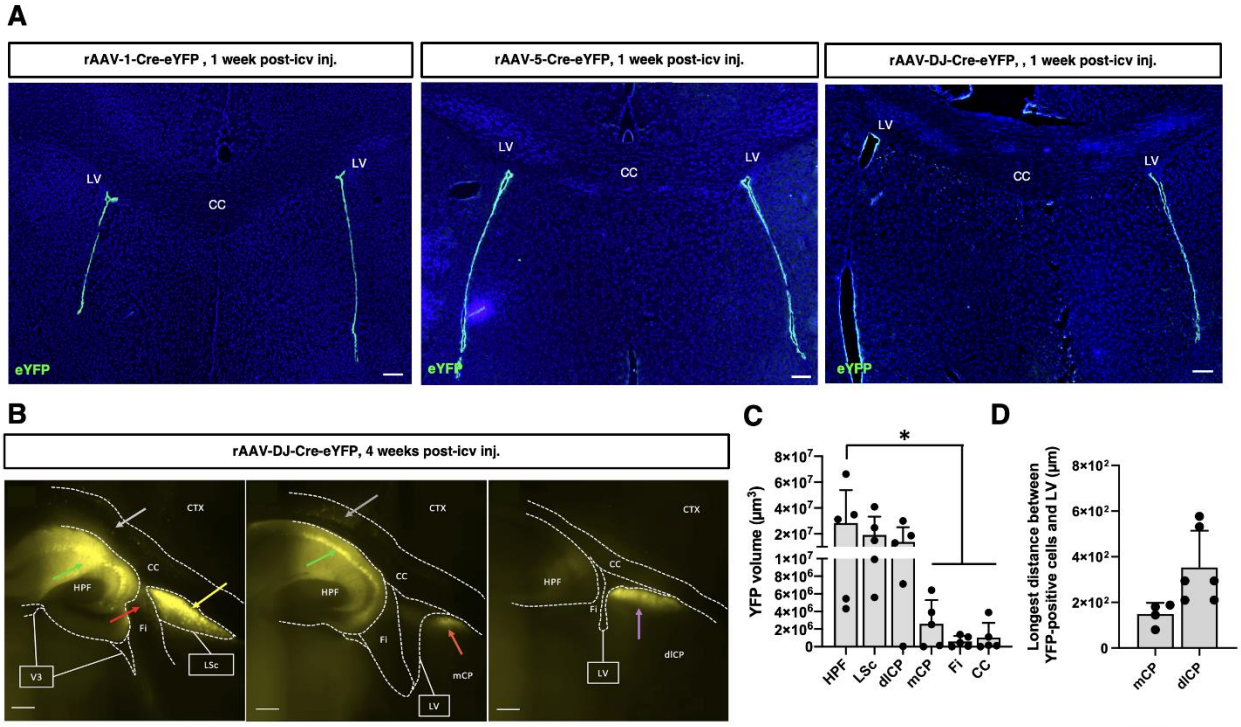

Figure 4

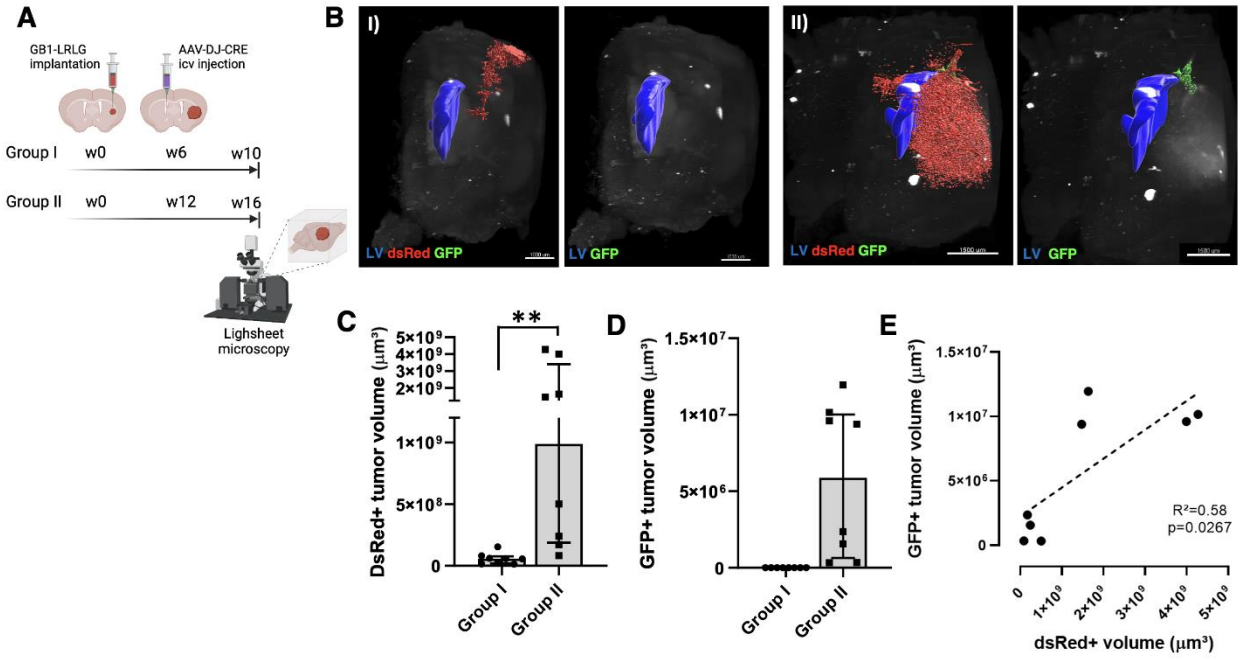

Figure 5

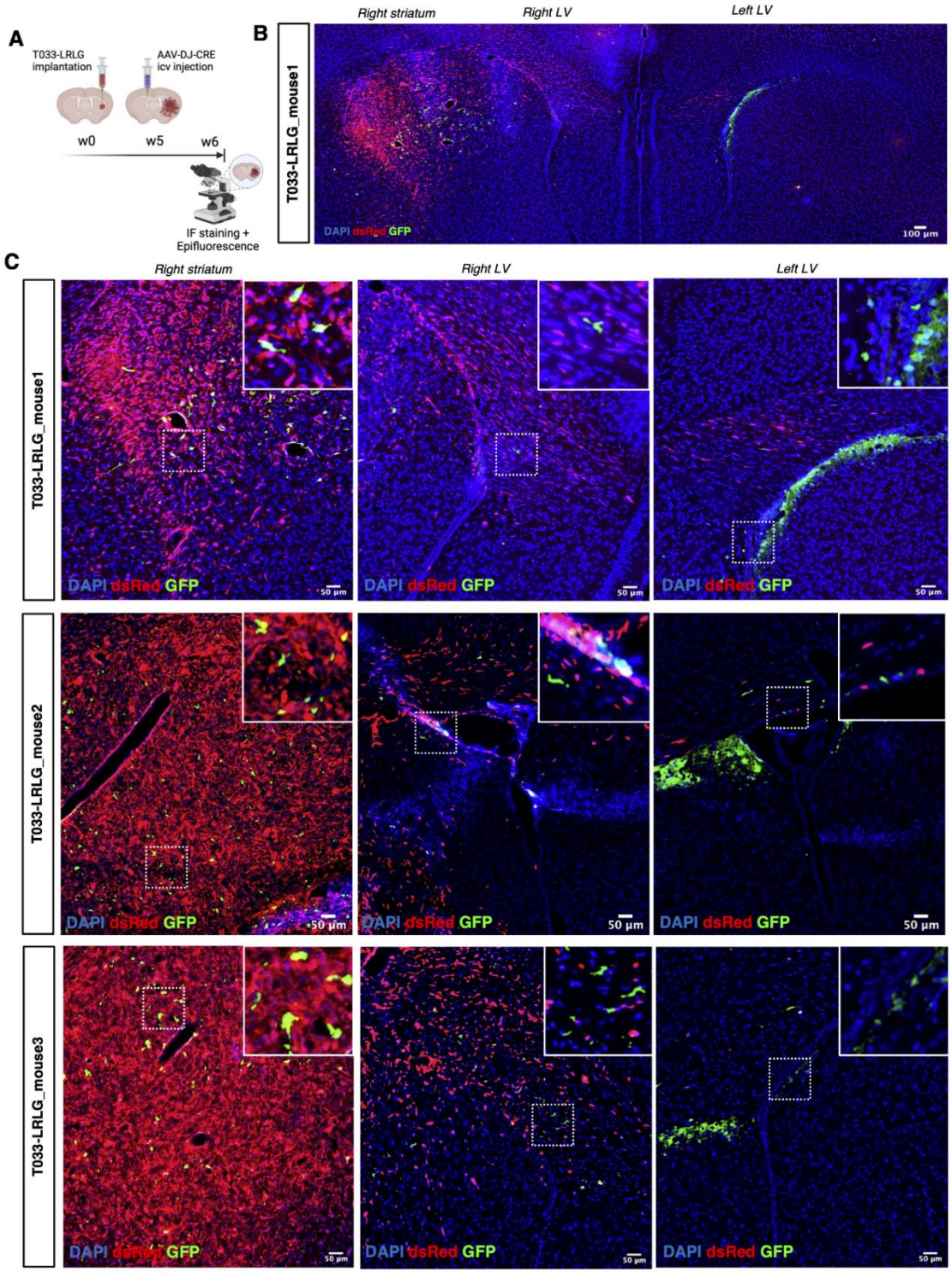

Figure 6